Study of radiation and MHD instability as a result of full impurity Shattered Pellet Injection by non-linear 3D JOREK simulation

6th Theory and Simulation of Disruptions Workshop 2018-07-16

Di Hu (胡地, Di.Hu@iter.org)
Collaborators: E. Nardon, G.T.A. Huijsmans, M. Lehnen, D. van Vugt.

Science Division, ITER Organisation
Route de Vinon-sur-Verdon,CS 90 046, 13067 St. Paul-lez-Durance, France
The views and opinions expressed herein
DO NOT necessarily reflect those of the ITER organization.

6th TSDW
2018 July, Princeton, NJ

Abstract

- The impurity radiation and ensuing large scale MHD instability caused by full impurity Shattered Pellets Injection (SPI) for the thermal quench (TQ) mitigation are investigated in this study.
- Compared with the deuterium SPI, evident global current contraction occurs due to much stronger radiative cooling.
- Both the $n = 0$ current profile contraction and the helical cooling effect play important roles in the MHD excitation.
- Strong asymmetry of the radiation profile in both toroidal and poloidal direction is identified. Such asymmetry is caused by the competition between local fragment ablation and parallel impurity density relaxation. Both asymmetry gradually relax after the TQ.
- The impurity radiation is able to deplete more than 80% of the pre-injection thermal energy even for the smallest caliber JET SPI.
- The impact of several injection parameters on the radiation and the MHD activities is shown.

Contents

Introduction to the impurity SPI

- The Shattered Pellet Injection (SPI) is part of the ITER disruption mitigation baseline concept both for the thermal quench (TQ) and the current quench (CQ) mitigation.
- For the TQ mitigation. Injection of impurity shattered pellet right before the thermal quench aims to mitigate the localized thermal load on the Plasma Facing Components (PFC) by radiatively dissipate the stored thermal energy uniformly onto the first wall.
- Such injection will also help to accelerate the current quench.
- The interplay between the radiative cooling and the MHD activity is important. The impurity SPI perturb the current profile by intense cooling from radiation and ablation, while the MHD dynamics governs how the thermal energy confinement is lost and how impurities are transported.
- Better understanding is required to achieve more efficient depletion of the thermal energy.

M. Lehnen, K. Aleynikova, P.B. Aleynikov et al., J. Nucl. Mater., **463**, 39-48 (2015)

Framework of the impurity SPI model

We consider the 3D reduced MHD where all species (including all charge states of the impurity) share a collective velocity field under strong charge exchange and strong inter-species friction assumption.

$$\mathbf{B} = F_0 \nabla\phi + \nabla\psi \times \nabla\phi, \tag{1}$$

$$\mathbf{v} = \mathbf{v}_\perp + v_\parallel \mathbf{B} = R^2 \nabla\phi \times \nabla u + v_\parallel \mathbf{B}. \tag{2}$$

Using $\{f, g\} \equiv R(\nabla f \times \nabla g) \cdot \nabla\phi$, the governing equations are then:

$$\frac{\partial \psi}{\partial t} = \eta(T)\Delta^*\psi - R\{u, \psi\} - F_0 \frac{\partial u}{\partial \phi}, \tag{3}$$

$$j = \Delta^*\psi, \quad j_\phi = -j/R, \tag{4}$$

$$\begin{aligned} R\nabla \cdot \left[R^2 \nabla_{pol} \frac{\partial}{\partial t} \rho u\right] = & \frac{1}{2}\left\{R^2 \left|\nabla_{pol} u\right|^2, R^2 \rho\right\} + \left\{R^4 \rho\omega, u\right\} \\ & - R\nabla \cdot \left[R^2 \nabla_{pol} u \nabla \cdot (\rho \mathbf{v})\right] + \{\psi, j\} - \frac{F_0}{R}\frac{\partial j}{\partial \phi} \\ & + \left\{P, R^2\right\} + R\mu(T_e)\nabla^2_{pol}\omega, \end{aligned} \tag{5}$$

Framework of the impurity SPI model (cont.)

Continuing from the previous slide,

$$\omega = \frac{1}{R}\frac{\partial}{\partial R}\left(R\frac{\partial u}{\partial R}\right) + \frac{\partial^2 u}{\partial Z^2}, \tag{6}$$

$$\frac{\partial}{\partial t}\rho = -\nabla\cdot(\rho\mathbf{v}) + \nabla\cdot\left[D_D\nabla\left(\rho-\rho_{imp}\right)\right] + \nabla\cdot\left(D_{imp}\nabla\rho_{imp}\right) + S_D + S_{imp}, \tag{7}$$

$$\begin{aligned}\frac{\partial P}{\partial t} &= -\mathbf{v}\cdot\nabla P - \gamma P\nabla\cdot\mathbf{v} + \frac{2}{3R^2}\eta\left(T_e\right)j^2 + \nabla\cdot\left(\kappa_\perp\nabla_\perp T + \kappa_\parallel\nabla_\parallel T\right)\\ &\quad - n_e n_{imp} P_{rad}\left(T_e\right) - \partial_t E_{ion},\end{aligned} \tag{8}$$

$$\begin{aligned}B^2\frac{\partial}{\partial t}\left(\rho v_\parallel\right) &= -\frac{1}{2}\rho\frac{F_0}{R^2}\frac{\partial}{\partial\phi}\left(v_\parallel B\right)^2 - \frac{\rho}{2R}\left\{B^2 v_\parallel^2,\psi\right\} - \frac{F_0}{R^2}\frac{\partial P}{\partial\phi} + \frac{1}{R}\left\{\psi,P\right\}\\ &\quad - B^2\nabla\cdot(\rho\mathbf{v})\,v_\parallel + B^2\mu_\parallel\left(T_e\right)\nabla_{pol}^2 v_\parallel,\end{aligned} \tag{9}$$

$$\frac{\partial}{\partial t}\rho_{imp} = -\nabla\cdot\left(\rho_{imp}\mathbf{v}\right) + \nabla\cdot\left(D_{imp}\nabla\rho_{imp}\right) + S_{imp}. \tag{10}$$

Here, $P \equiv m_D^{-1}\left(\rho + \alpha_{imp}\rho_{imp}\right)T$, with $\alpha \equiv -1 + \left(\langle Z\rangle_{imp} + 1\right)m_D/2m_{imp}$, $T = 2T_e$ and P_{rad} is the radiative cooling rate. Two more components are needed in order to construct the model, namely the deuterium and impurity source and the local charge state distribution of the impurity.

The Neutral Gas Shielding model

- The ablation of pellets in a Maxwellian plasma is considered by using the strong neutral gas shielding (NGS) model,

$$\partial_t N\left[\frac{atom}{s}\right] \simeq 1.94\times 10^{14} n_e^{0.45}\left[cm^{-3}\right] T_e^{1.72}\left[eV\right] r_p^{1.44}\left[cm\right] A_p^{-0.28} Z_p^{-0.56}\left(\gamma-1\right)^{0.28}. \quad (11)$$

- Energetic ions result in enhanced ablation, while runaway electrons result in volume heating. Both are not considered in our study.

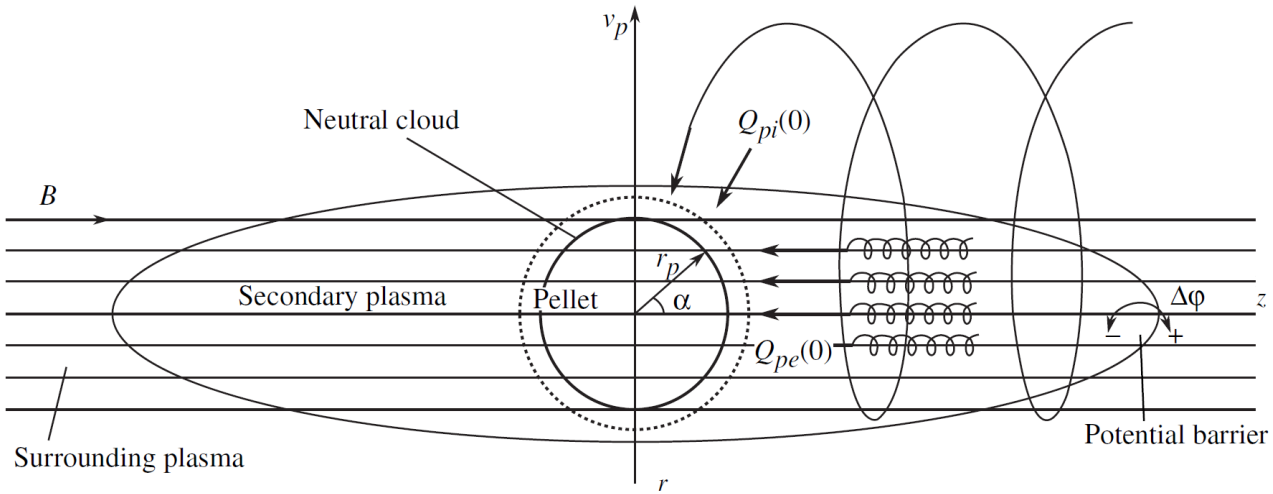

V. Yu. Sergeev et al., Plasma Physics Reports, 2006; Pégourié et al., Plasma Phys. Control. Fusion, 2005.

The Statistical Fragmentation model

The fragment shard size distribution is modelled according to the Statistical Fragmentation model which shows remarkable agreement with the laboratory fragment size distribution from the fast camera data.

$$P(r_p) = \frac{r_p K_0(\kappa_p r_p)}{I}, \quad I \equiv \int_0^\infty r_p K_0(\kappa_p r_p)\, dr = \kappa_p^{-2}, \tag{12}$$

where K_0 is the modified Bessel function of the second kind.

- The atom number contained within each fragment goes up with $N \propto r_p^3$
- The ablation rate goes up with $\partial_t N \propto r_p^{1.44}$.
- The large ones survive much deeper than the smaller ones.

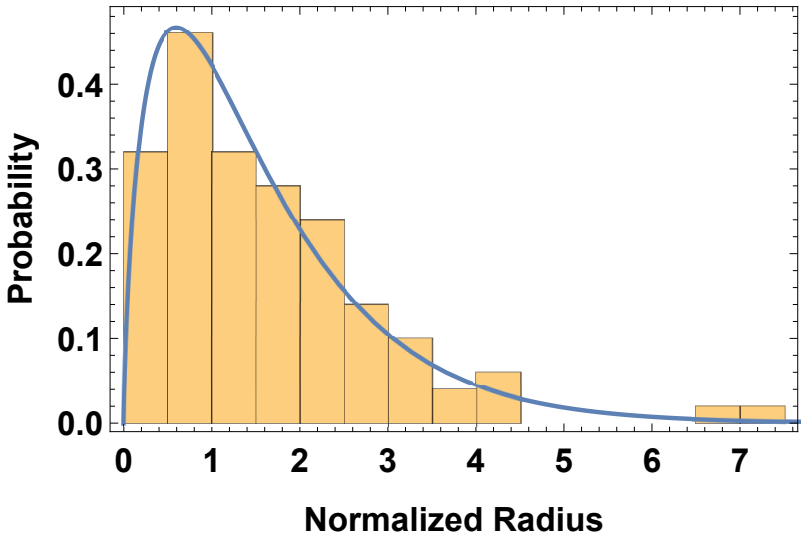

P. Parks, GA report GA-A28352, 2016; L. Baylor et al., PPPL TSD workshop report, 2017

The Coronal Equilibrium assumption

- The plasma during a injection is **not** in a Coronal Equilibrium (CE).
- The deviation in radiation is small for a rapidly cooling plasma.
- We compare the CE result, in 0D, against a time evolving model with convective loss and neutral source in a cooling plasma (exponentially cooled from $5keV$ to $10eV$ with timescale $\tau_{cool} \sim 10^{-5}s$).

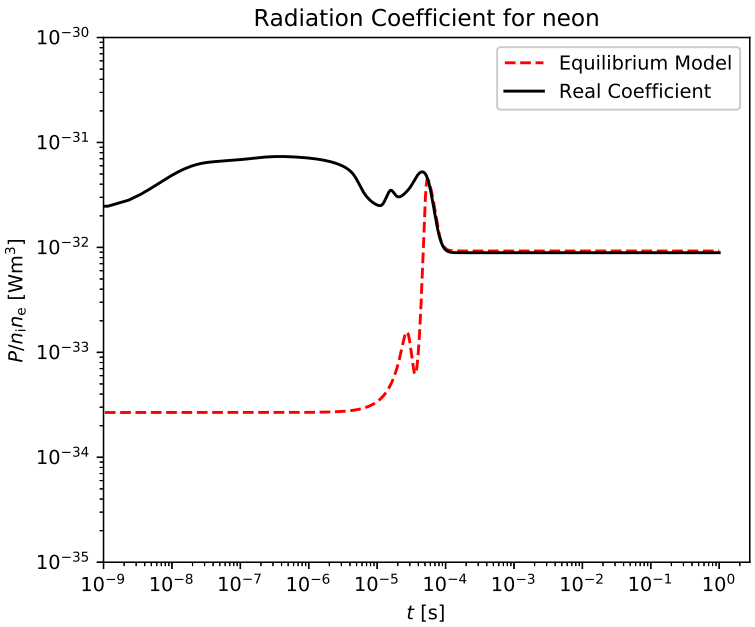

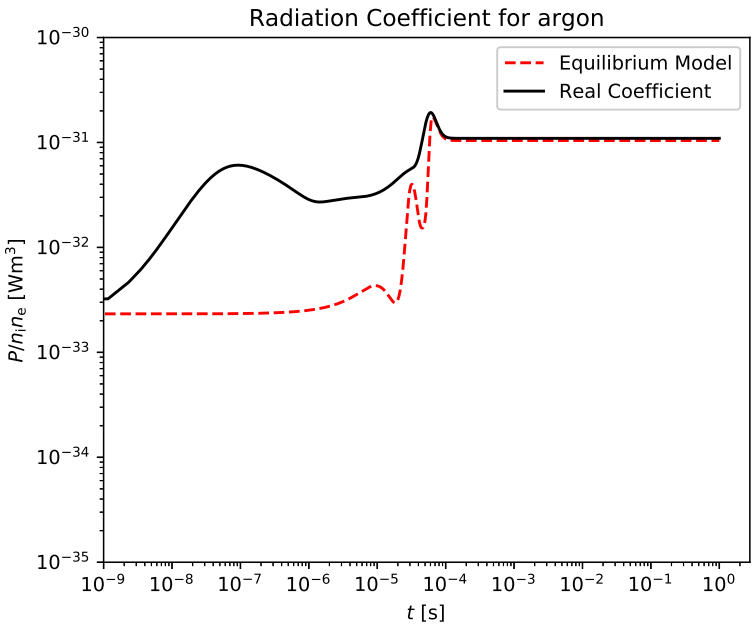

Target equilibrium before injection

JET shot 85943 at time $62.4s$ is used as the target equilibrium. Toroidal field $B_t = 3T$, plasma current $I_p = 2MA$, thermal energy $W_{th} \simeq 0.5MJ$.

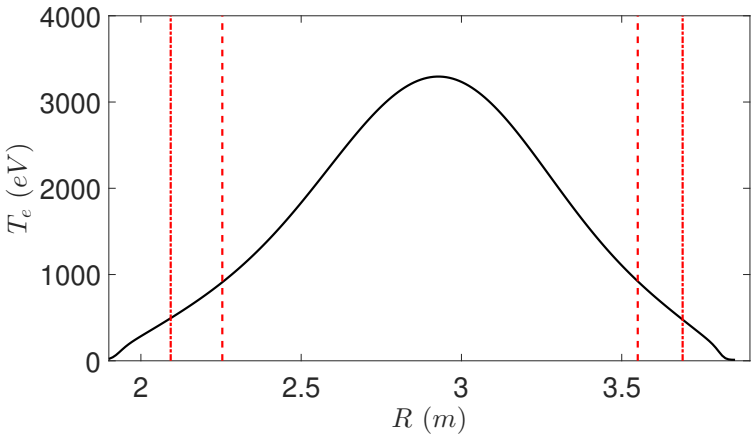

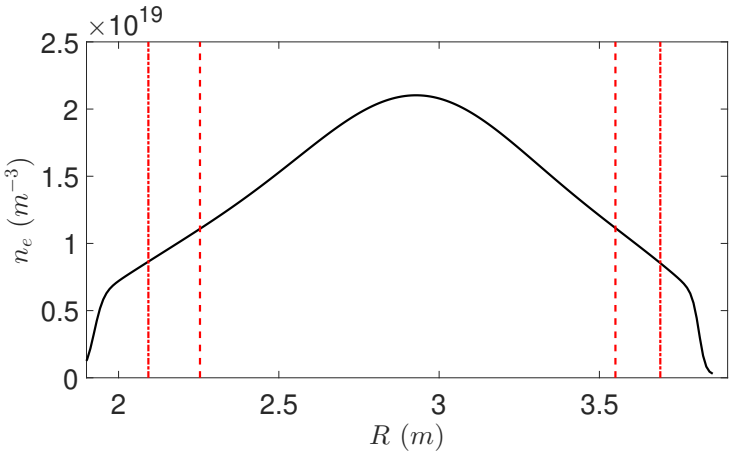

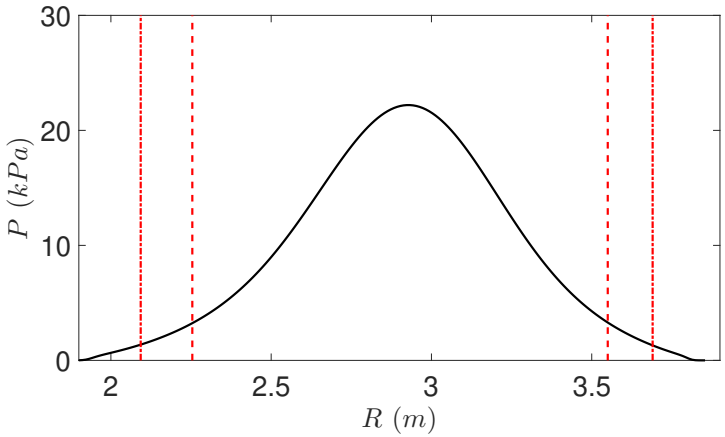

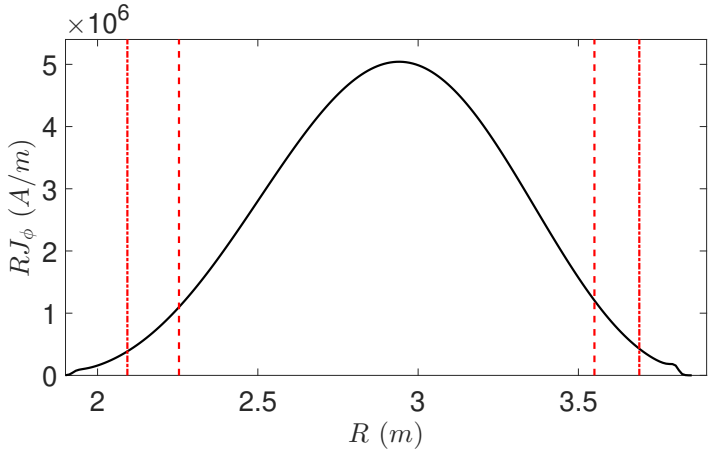

Initial q profile before injection

The $q = 2$ surface is far away from the ideal wall, and it can be expected that $2/1$ resistive kink can go unstable once significant amount of current is squeezed within $q = 2$ surface. The $q = 1$ surface is almost non-existent in this particular case.

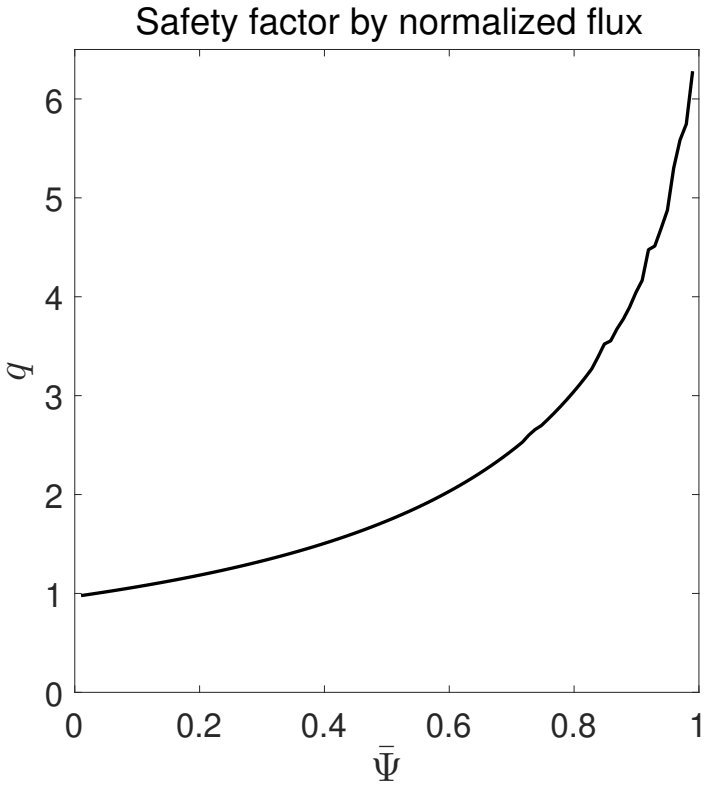

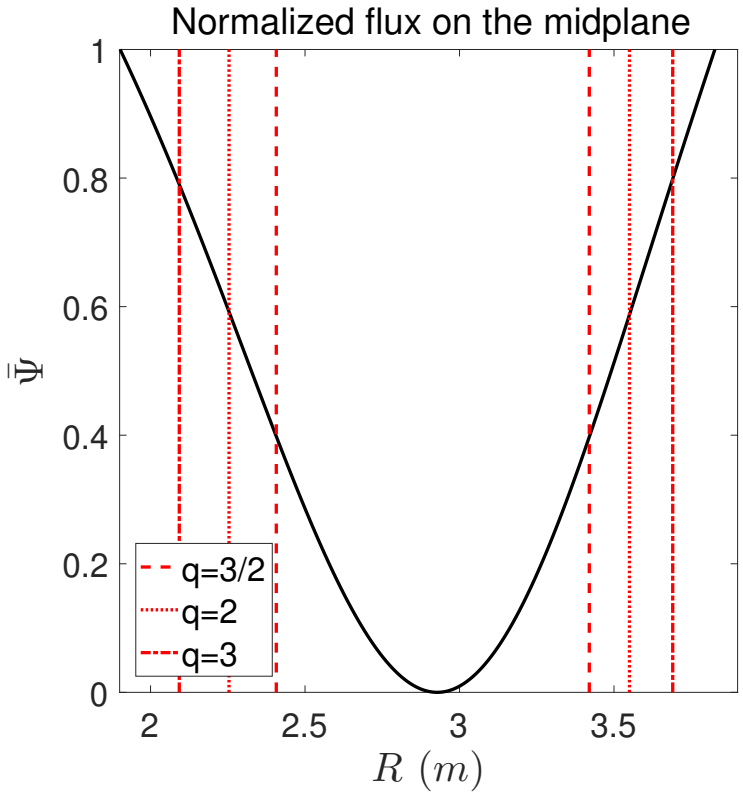

Injection configuration

- The axis of the injection cone lies within the (R, Z) plane, with a vertex 20 degrees, resembling that of the upcoming JET system.
- The speed spread is 40% of the reference injection speed, with flat probability function. The pellet is shattered into 100 fragments, with characteristic fragment size $0.25mm$.
- Three calibers of SPI is available for the future JET system.

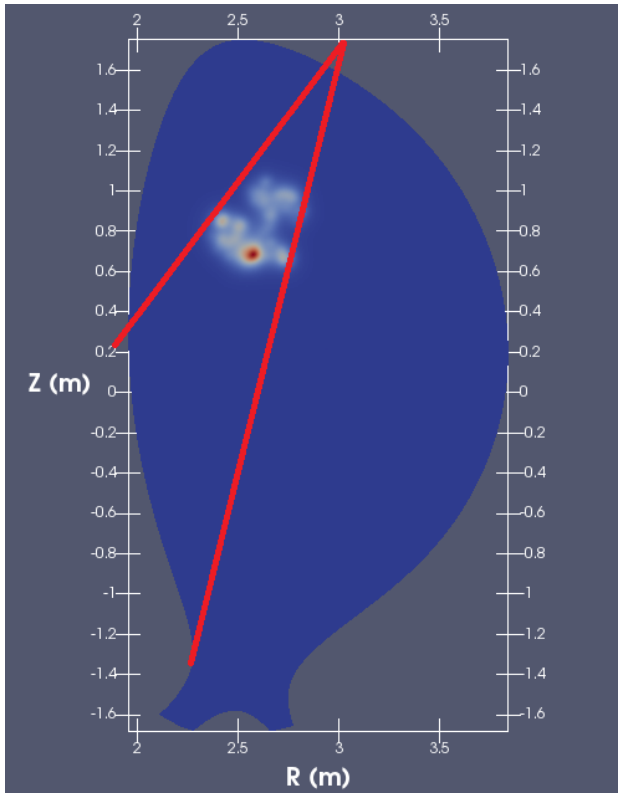

Barrel No	Diameter [mm]	Length [mm]	Expected range of pellet speed [m/s]	Punch	Ar quantity	Ne quantity	D2 quantity
1	12.5	31.25	150-200	Yes	$9x10^{22}$	$1.6x10^{23}$	$2.3x10^{23}$
2	8.0	12.0	150-200	Yes	$1.5x10^{22}$	$2.6x10^{22}$	$3.6x10^{22}$
3	4.5	5.8	250-500	No	-	$4.0x10^{21}$	$5.6x10^{21}$

Radiative cooling by impurity SPI

- A neon small caliber SPI is used to demonstrate the radiative cooling.
- The temperature profiles are shown for $0.0ms$, $1.19ms$, $1.31ms$ (just after the TQ) & $1.36ms$, respectively.
- Before the TQ, the T_e in the wake of the fragments are down to the order of $10eV$, until the TQ occurs and the outgoing heat flux re-heat the plasma.

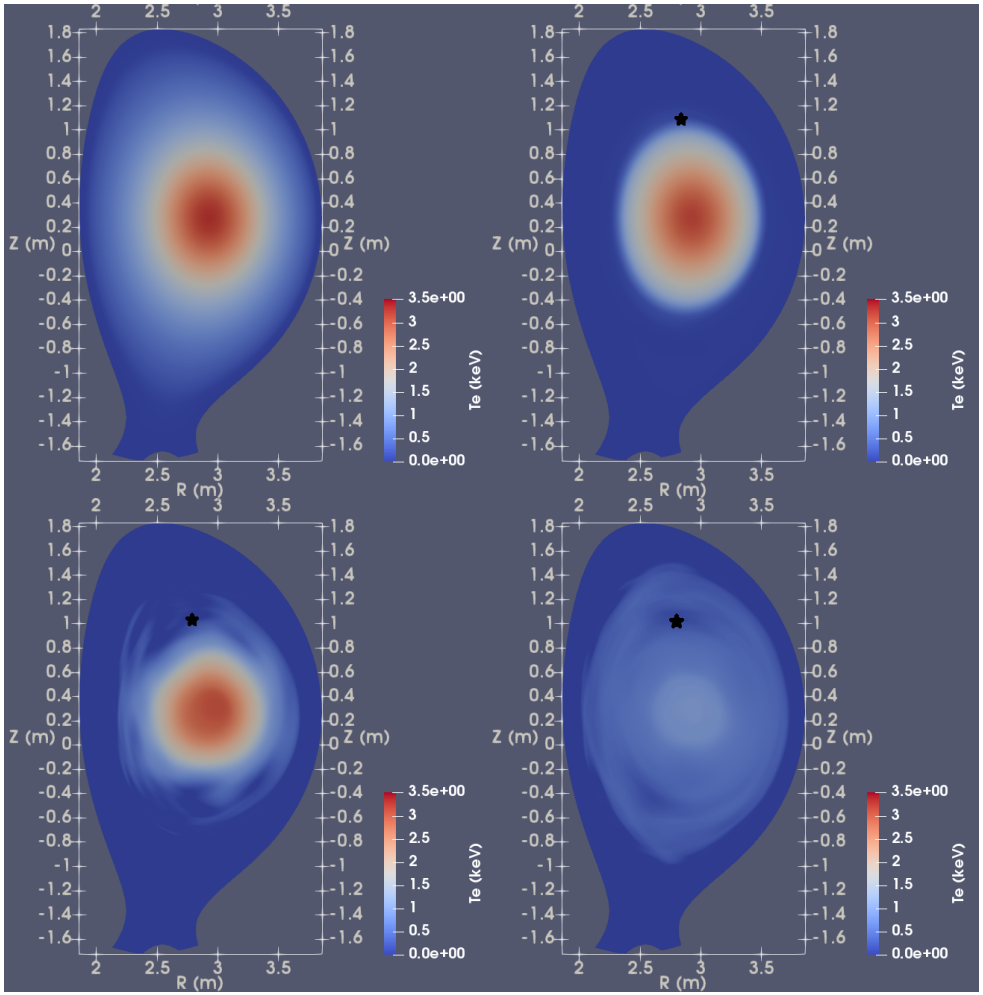

$n = 0$ current contraction

- Evident $n = 0$ current profile contraction occurs before the TQ. The TQ is triggered when the cooling front (thus the fragments) and the current channel boundary enter the $q = 2$ surface.
- Compared with the deuterium SPI, the much stronger current channel contraction is due to the much lower post-injection temperature ($\mathcal{O}(10eV)$ vs. $\mathcal{O}(100eV)$).

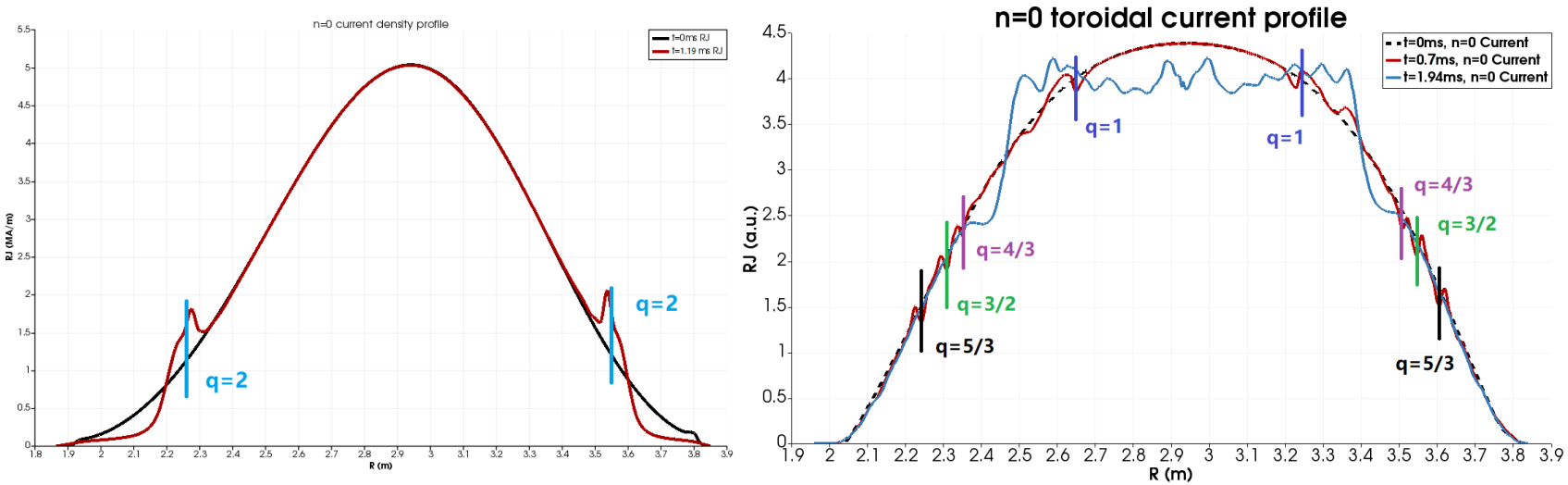

The $n = 0$ current profile for neon SPI (left) and deuterium SPI (right).

Helical cooling structure

Helical cooling effect exists during the whole process, both before and after the TQ, though the latter seems to be more prominent.

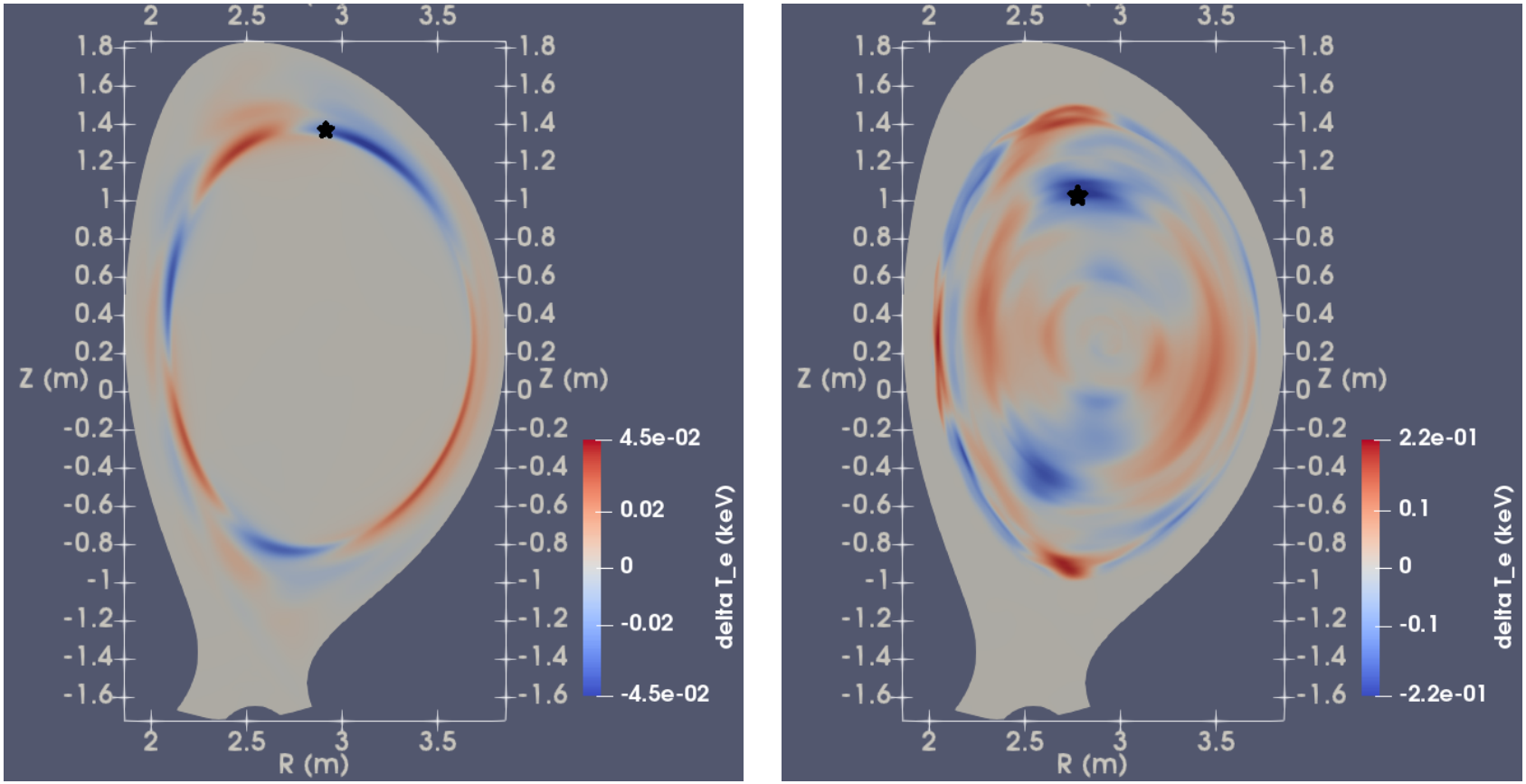

The perturbed temperature profile for $0.59ms$ (before the TQ) & $1.36ms$ (after the TQ), respectively.

Competition between the two mechanisms

- The competition between those two mechanism is governed by the comparison of the global current contraction timescale and the pellets travel timescale.
- If the global current contraction time is quick comparing with pellets travel time, the contraction follows closely with the shards, and little current density is left to be disturbed locally.
- After the TQ, however, due to the relaxation of the temperature and the current profile, the $n = 0$ contribution vanishes.

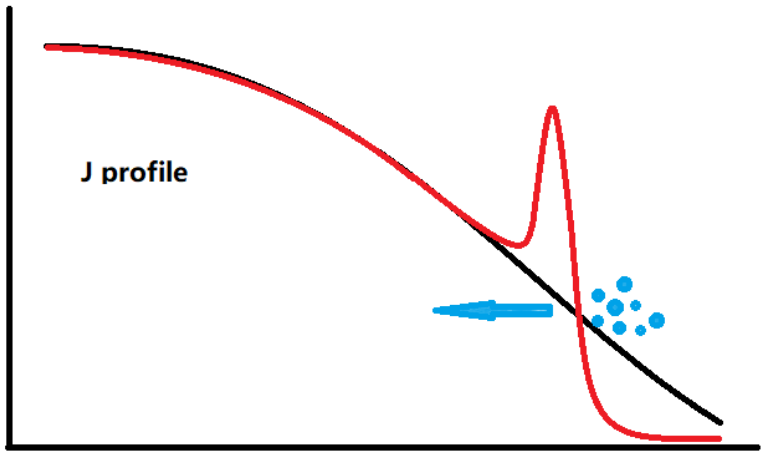

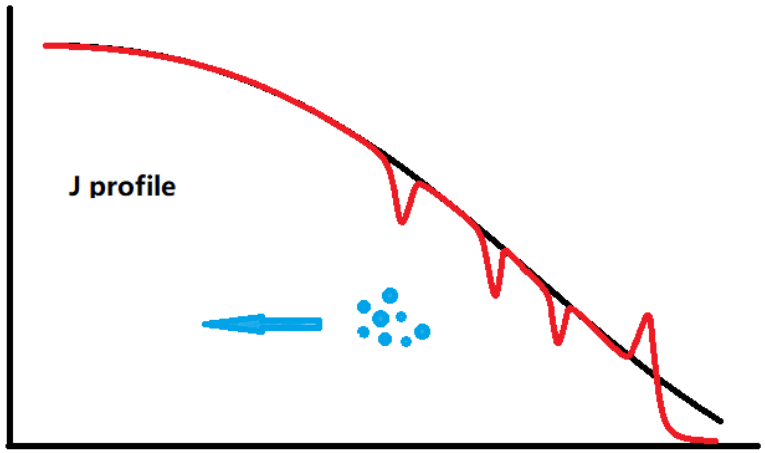

MHD spectrum

- Low perturbation level before the fragments approach the $q = 2$.
- Sudden growth of modes as the current channel goes into the $q = 2$.
- Collective growth of modes results in wide spread stochasticity.

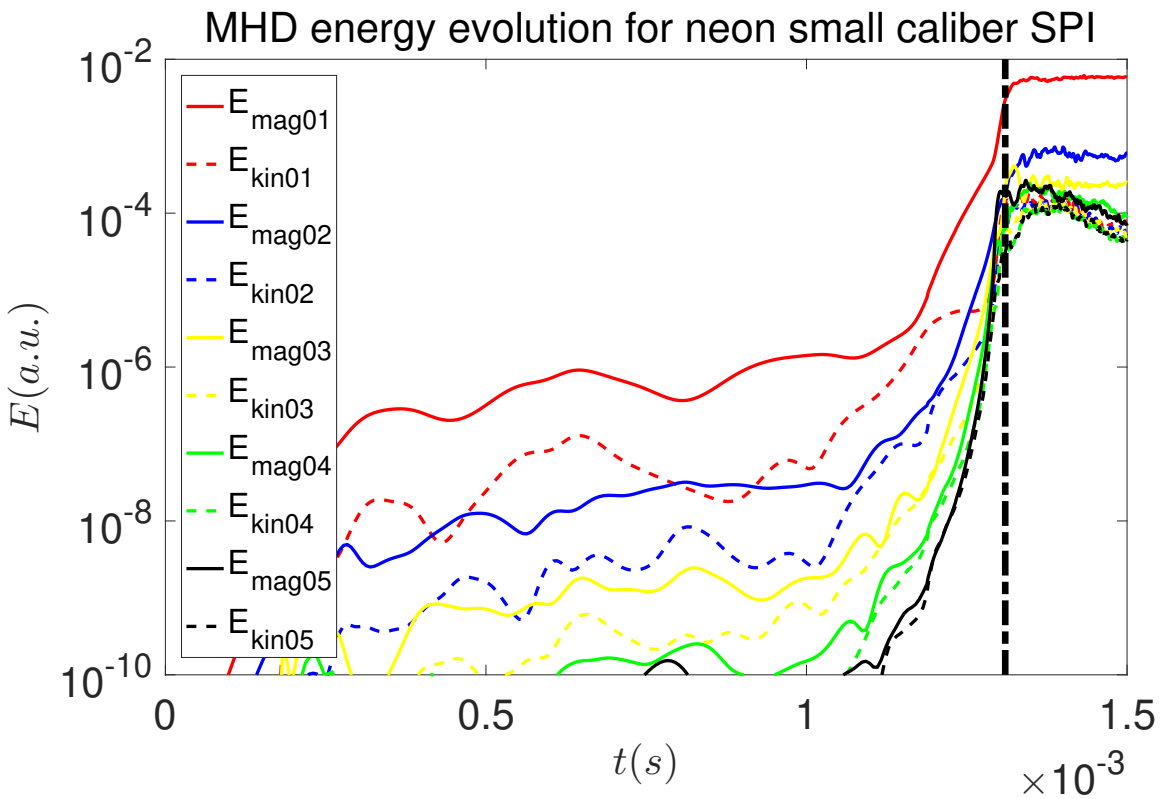

The Poincaré plot of magnetic field

- No wide-spread stochasticity before the TQ, the $n = 0$ contraction dominates over the helical cooling before the TQ.
- Field line stochasticity occurs across the whole plasma after the TQ.

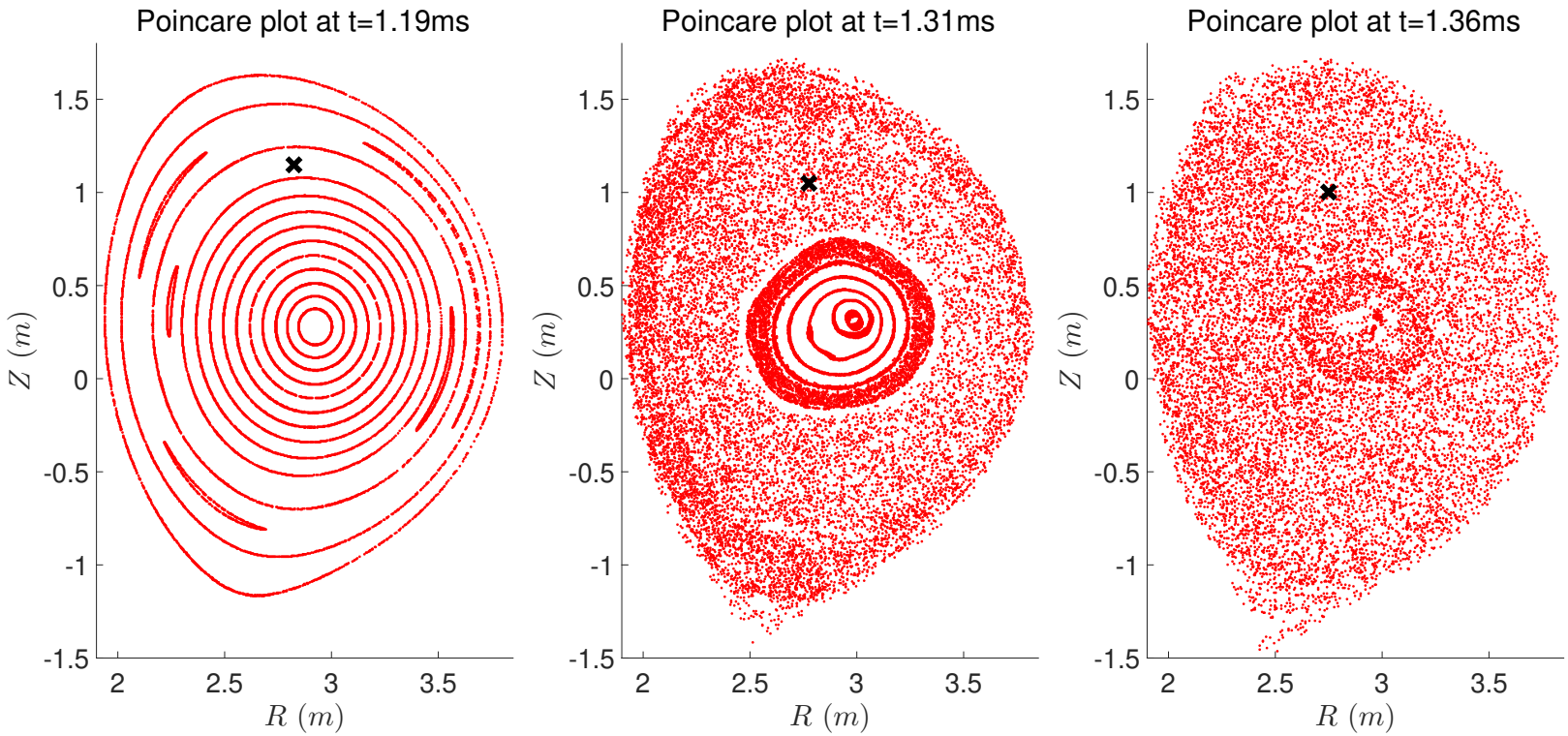

Pre-TQ MHD excitation

- Before approaching the $q = 2$ surface, rational surfaces are still destabilized as fragments (thus also the cooling front) travels inward.
- The destabilization not persistent compared with the deuterium case.

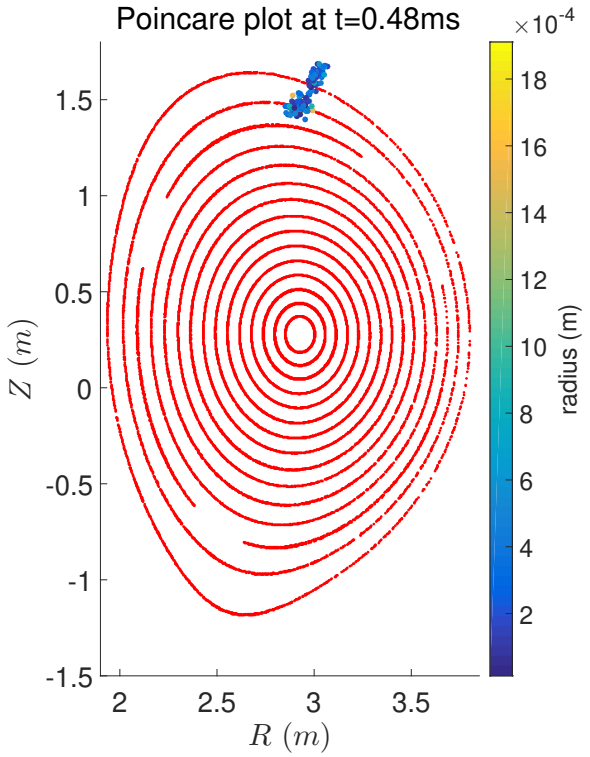

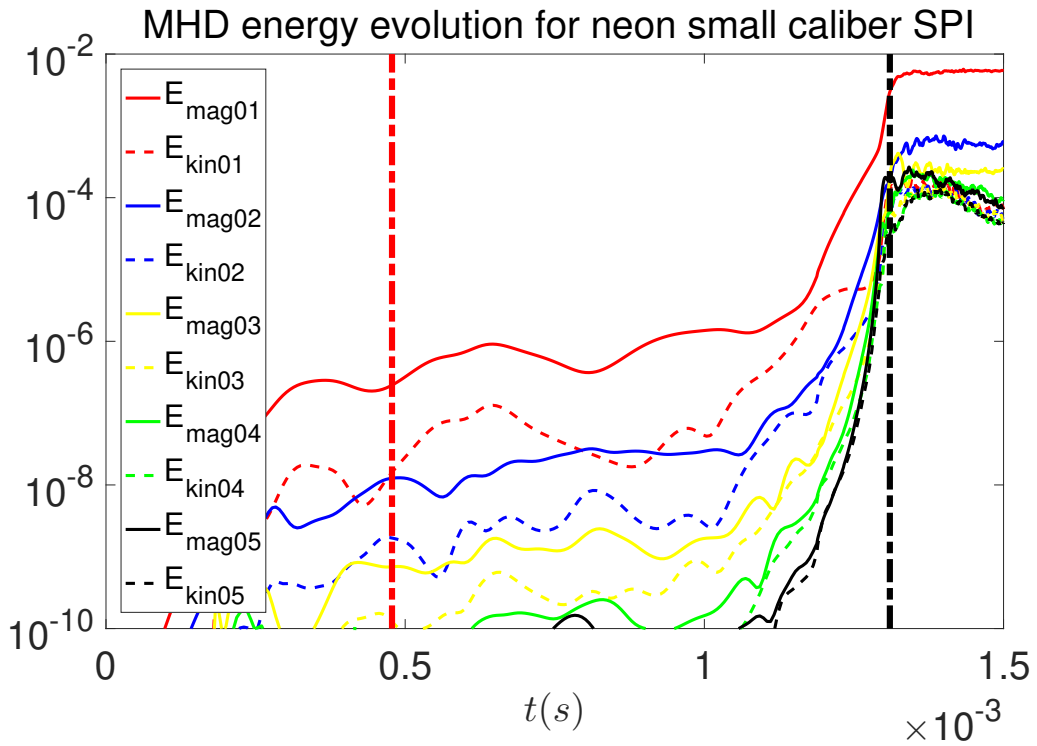

Pre-TQ MHD excitation (cont.)

- Cold post-injection plasma means insignificant helical cooling.
- Also little current is left to be perturbed locally.
- The lack of stochasticity beneficial for thermal energy mitigation.

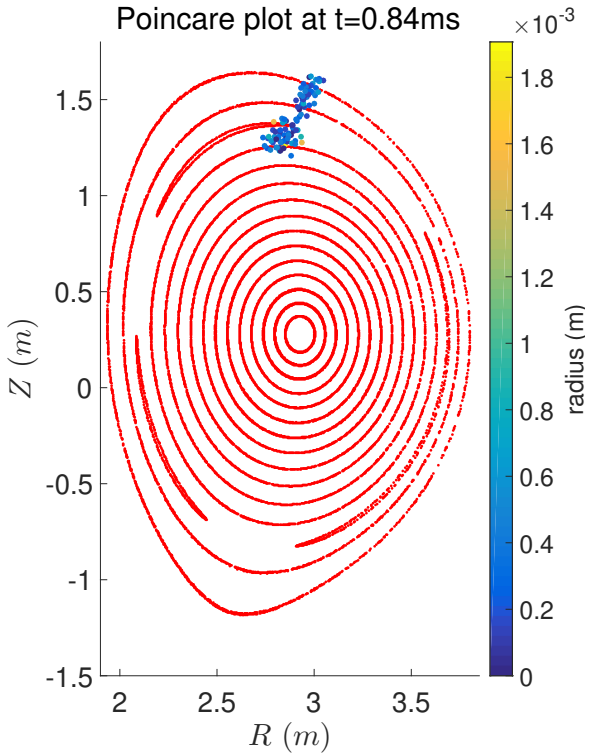

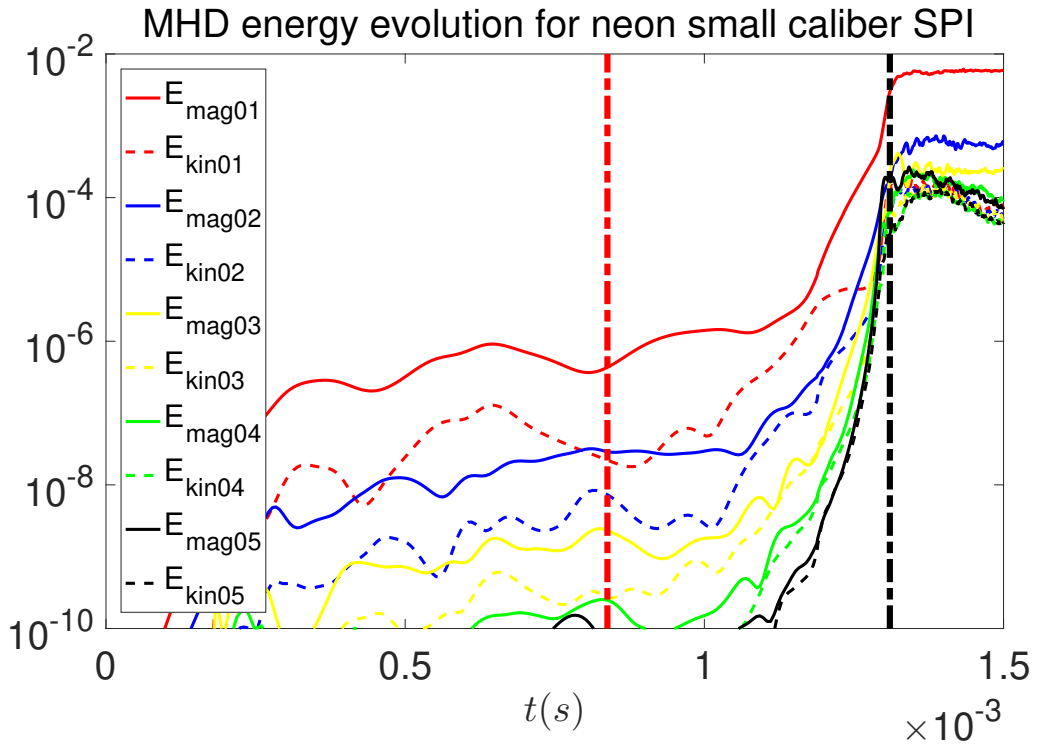

Pre-TQ MHD excitation (cont.)

- The $2/1$ mode, as well as its higher harmonics begin to grow as the fragments arrive in the $q = 2$ surface en masse.
- The phase of the island suggests $n = 0$ contraction is dominant.

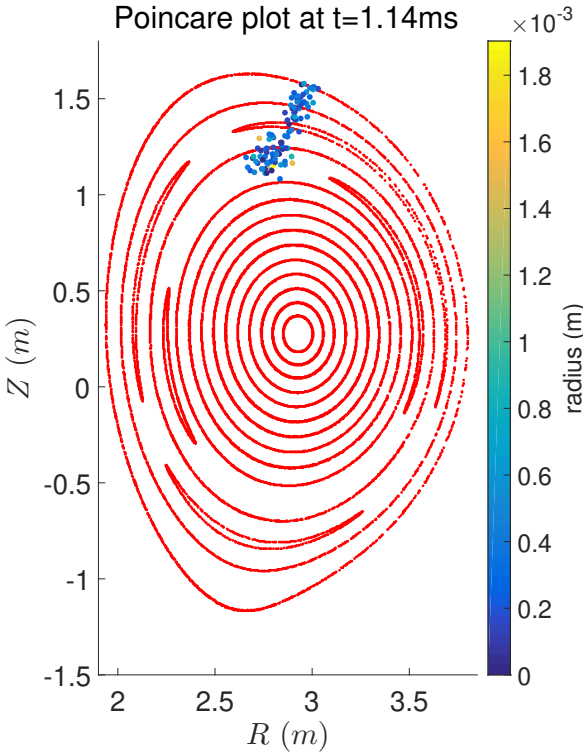

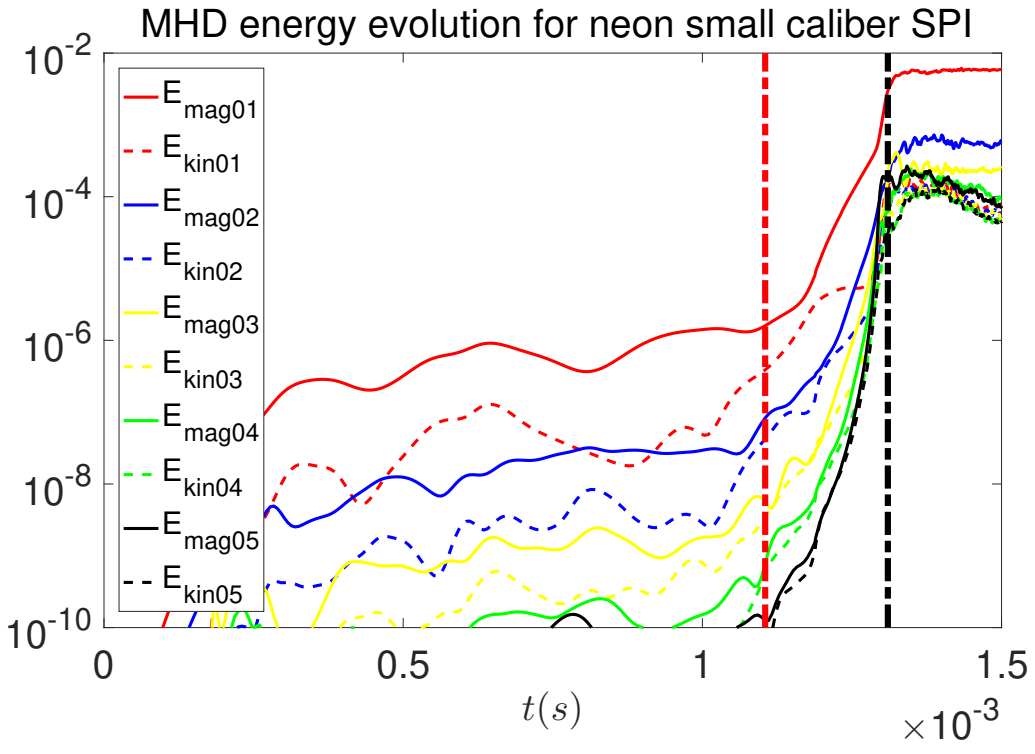

Dependence of q profile and injection configuration

- An alternative medium size equatorial SPI into the same equilibrium.
- Islands overlapping can occur if the cooling front is propagating fast enough between major rational surfaces.
- The exact behavior depends on the q profile, injection configuration and velocity although the destabilizing mechanisms remain the same.

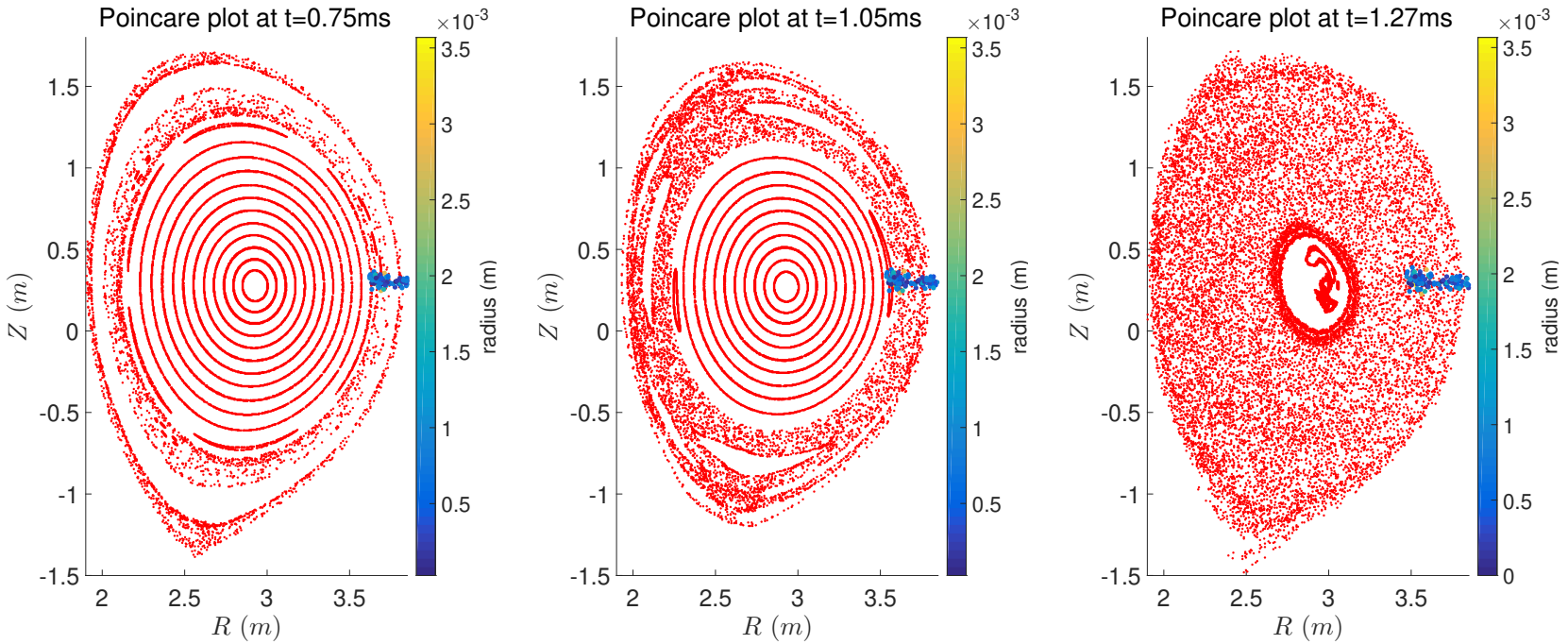

The poloidal asymmetry at injection location

- The electron temperature flattens quickly along the field line by parallel conduction.
- The radiation power density thus goes with $n_e n_{imp}$, while n_e is also dependent on n_{imp}, thus the power density estimately goes with n_{imp}^2.
- The poloidal asymmetry reflect the unrelaxed impurity density profile in poloidal plane.

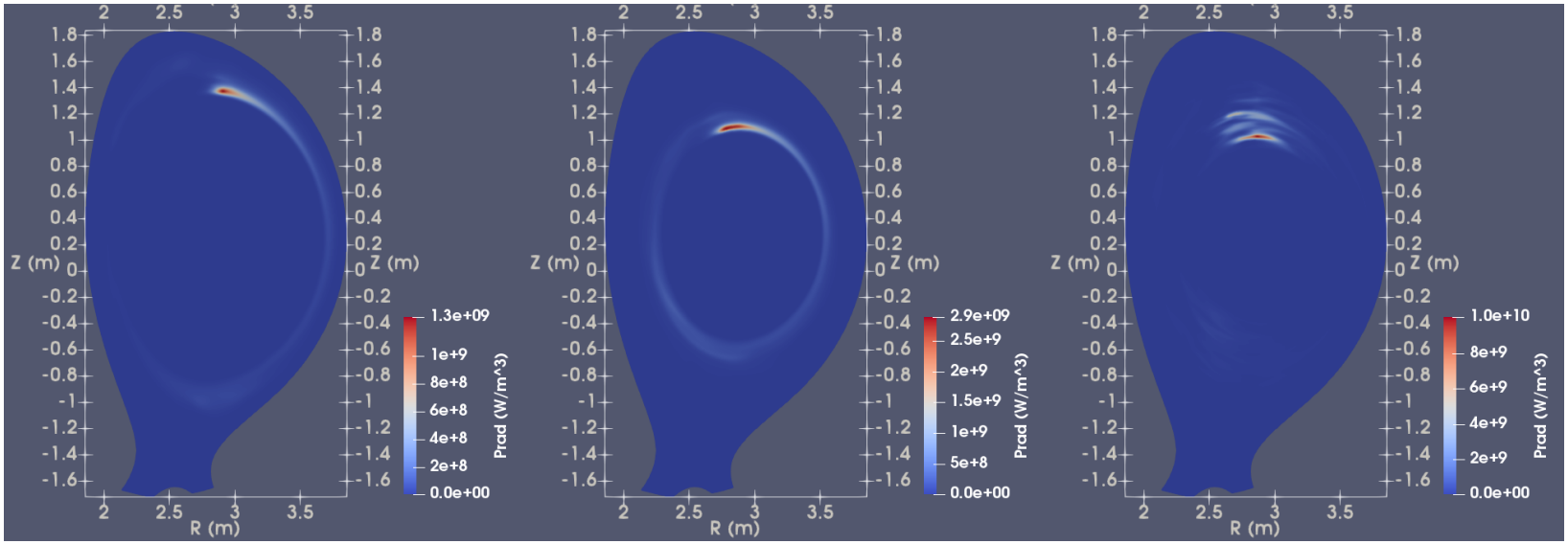

The radiation power density profile at SPI location for $0.59ms$, $1.19ms$, $1.36ms$, respectively.

The poloidal asymmetry $\pi/2$ away from the injection

- The poloidal asymmetry away from the injection location reflect the transformation surface the impurity density peak is on.
- We used a toroidally elongated impurity deposition, resulting in less poloidal asymmetry away from the injection than the realistic case.

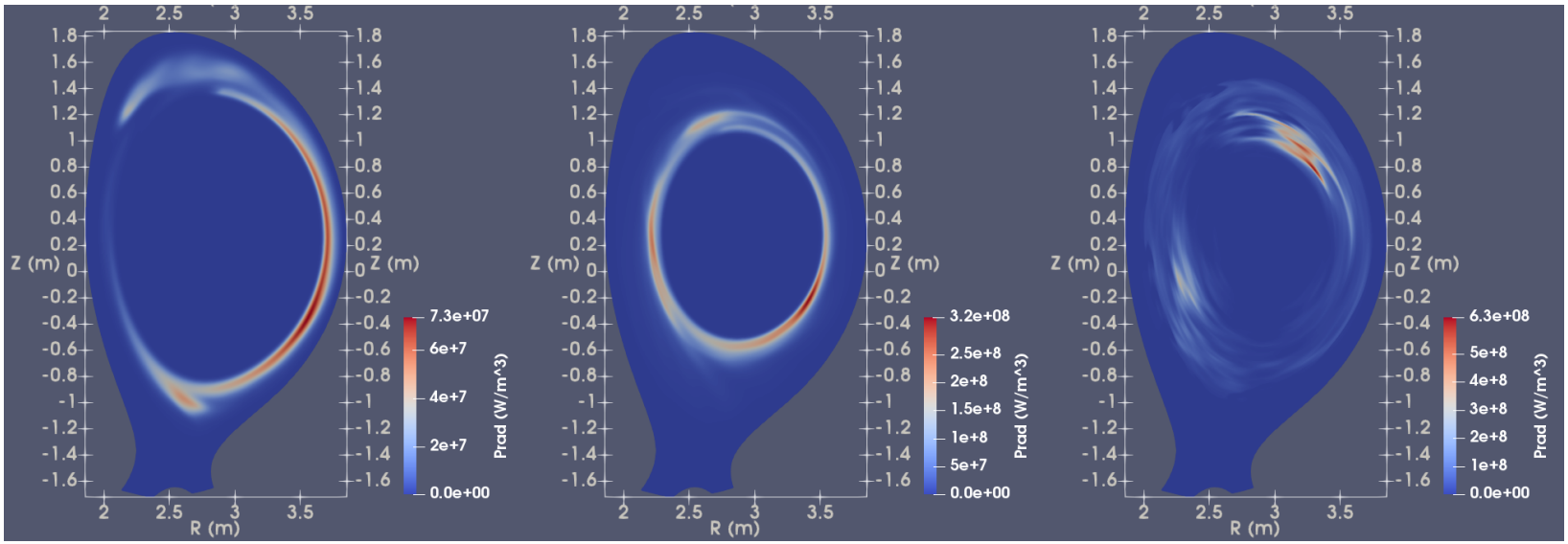

The radiation power density profile $\pi/2$ from SPI for $0.59ms$, $1.19ms$, $1.36ms$, respectively.

The poloidal asymmetry π away from the injection

- The poloidal asymmetry away from the injection location reflect the transformation surface the impurity density peak is on, thus keeps changing as the fragments goes in deeper.
- We used a toroidally elongated impurity deposition, resulting in less poloidal asymmetry away from the injection than the realistic case.

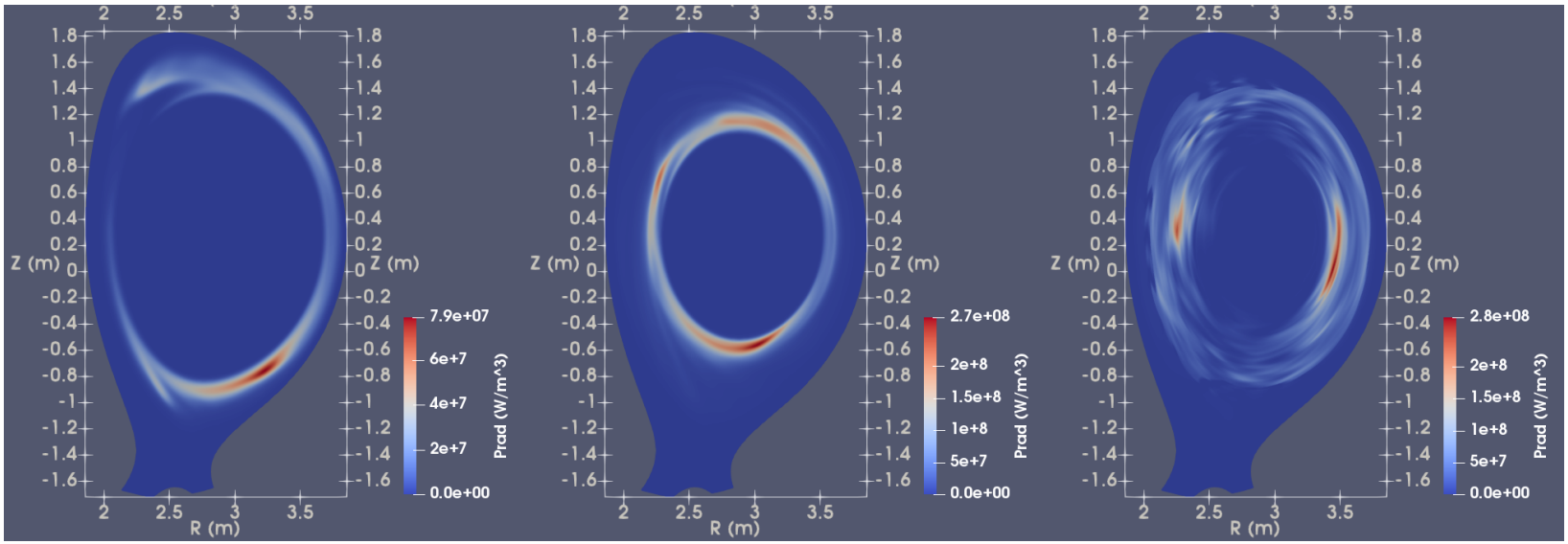

The radiation power density profile π from SPI for $0.59ms$, $1.19ms$, $1.36ms$, respectively.

The toroidal asymmetry

- The strong asymmetry along the field line direction is a result of the dynamic competition between the local ablation impurity source and the parallel sound speed impurity density relaxation.
- The toroidal asymmetry is more peaked than $n = 1$ as the power density goes with $n_e n_{imp}$.

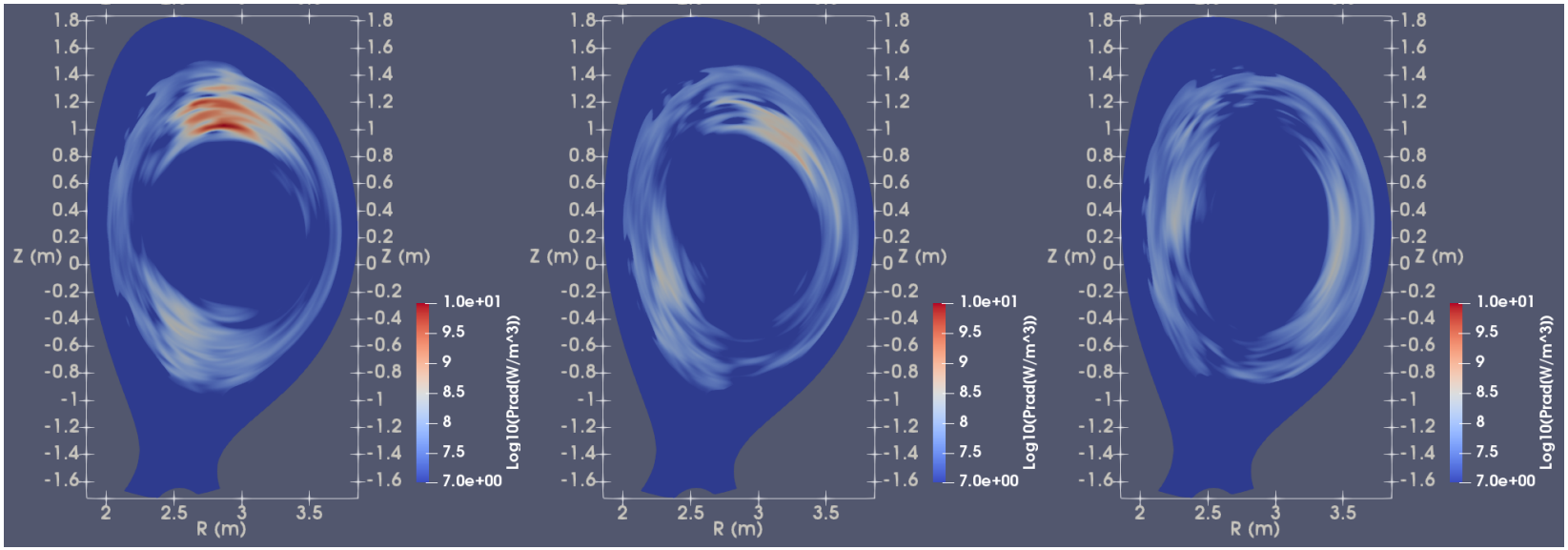

The $\log_{10}$ of radiation power density at $1.36ms$ for the above three toroidal location, respectively.

The toroidal asymmetry (cont.)

- The integrated radiation power within each poloidal plane still exhibit fairly strong toroidal asymmetry.
- The asymmetry is artificially mitigated by toroidal elongation of impurity deposition which is Gaussian-like with half-width radian 1.

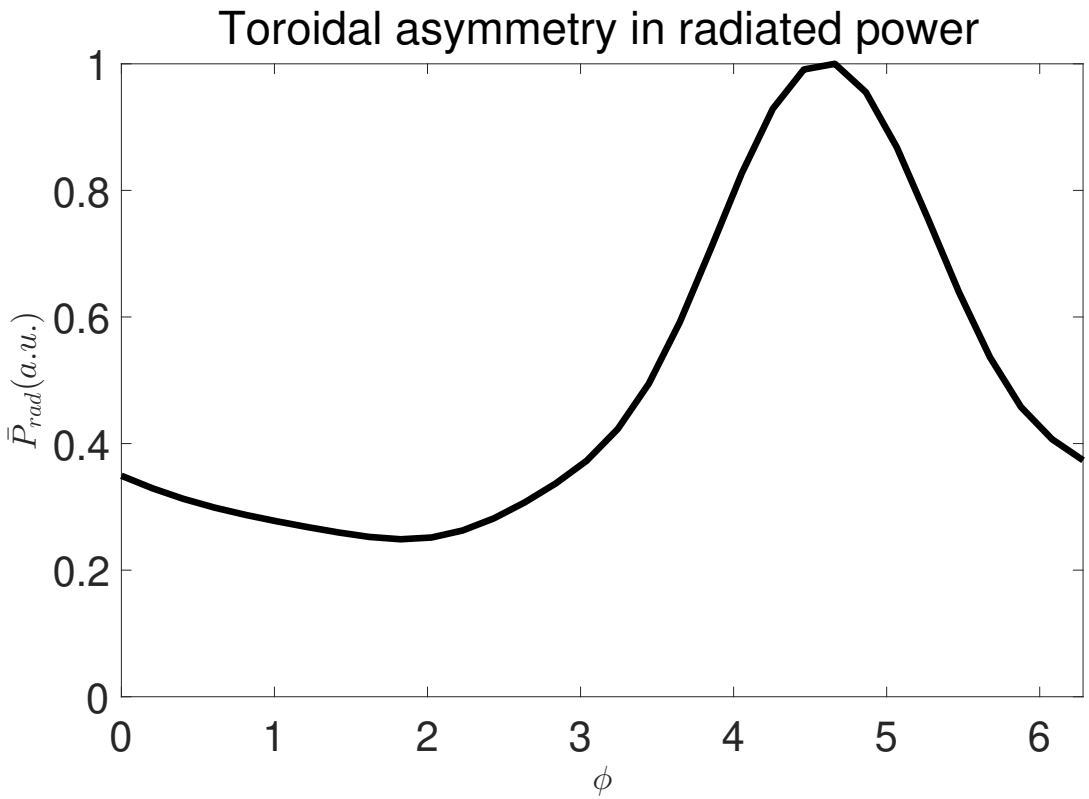

Total radiated energy

The impurity radiation dissipates more than 80% of the initial thermal energy at the end of the TQ (defined by most of the plasma cools down to $\mathcal{O}(10eV)$).

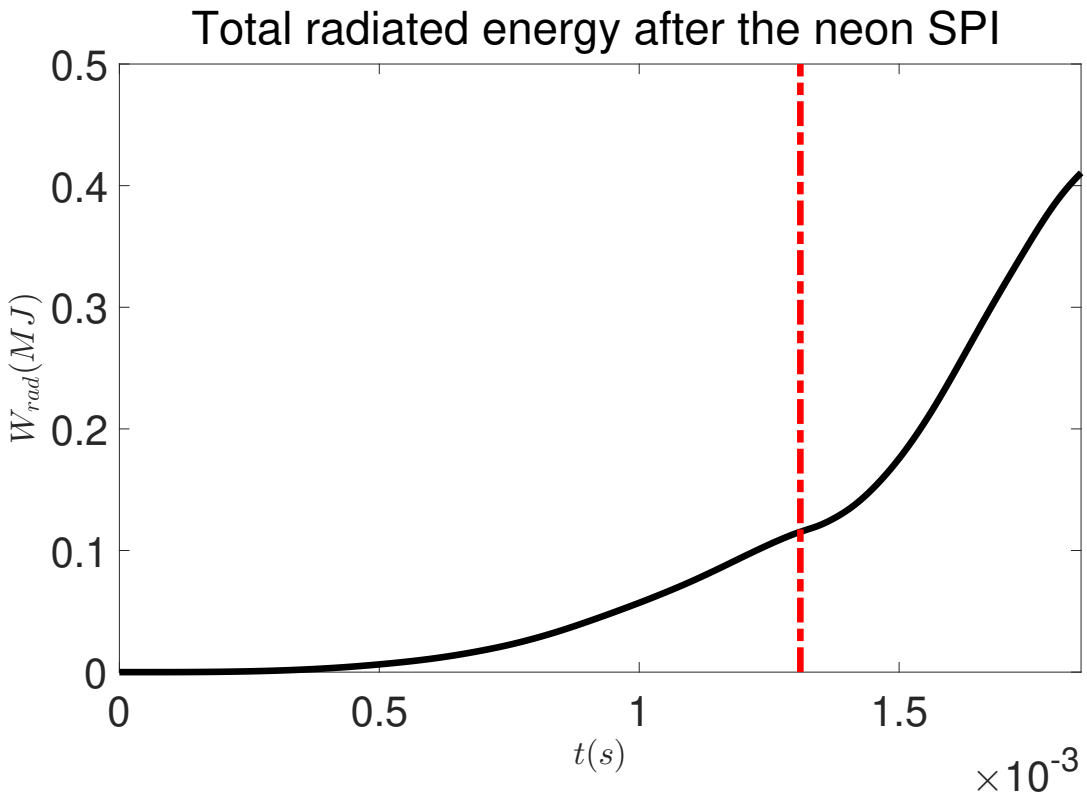

Conclusion

- MHD excitation by impurity SPI due to the $n = 0$ current shrinking and the helical effect.
- The TQ is triggered when the fragments (thus the cooling front) approach the $q = 2$ surface.
- Strong poloidal and toroidal asymmetry until hundreds of microseconds after the TQ onset.
- Away from the injection toroidal location, poloidal asymmetry changes over time.
- The toroidal peaking is stronger than $n = 1$.
- Radiation can dissipate most of the initial thermal energy even with small caliber SPI.